

Leveraging Co-Expression Network Analysis to Establish Transcriptional Shifts in the Gut of the Asian Citrus Psyllid During *Candidatus Liberibacter asiaticus* Infection [†]

Chang Chen ¹, Joshua B. Benoit ², Lukas A. Mueller ^{3,*} and Surya Saha ^{3,4,*}

¹ Department of Entomology, Cornell University, Ithaca, NY 14853; cc2589@cornell.edu

² Department of Biological Sciences, University of Cincinnati, Cincinnati, OH 45211; benoitja@ucmail.uc.edu

³ Boyce Thompson Institute, Ithaca, NY 14853

⁴ School of Animal and Comparative Biomedical Sciences, The University of Arizona, Tucson, AZ 85721

* Correspondence: lam87@cornell.edu, suryasaha@cornell.edu

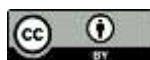
[†] Presented at the 1st International Electronic Conference on Entomology (IECE 2021), 1–15 July 2021;

Available online: <https://iece.sciforum.net/>.

Citation: Chen, C.; Benoit, J.B.; Mueller, L.A.; Saha S. Leveraging Co-Expression Network Analysis to Establish Transcriptional Shifts in the Gut of the Asian Citrus Psyllid During *Candidatus Liberibacter asiaticus* Infection, in Proceedings of the 1st International Electronic Conference on Entomology, 1–15 July 2021, MDPI: Basel, Switzerland, doi:10.3390/IECE-10515

Published: 1 July 2021

Publisher's Note: MDPI stays neutral with regard to jurisdictional claims in published maps and institutional affiliations.



Copyright: © 2021 by the authors. Submitted for possible open access publication under the terms and conditions of the Creative Commons Attribution (CC BY) license (<http://creativecommons.org/licenses/by/4.0/>).

Abstract: Asian citrus psyllid (ACP, *Diaphorina citri*) is the vector for the bacteria, *Candidatus Liberibacter asiaticus* (CLAs), that causes Huanglongbing (HLB, citrus greening disease). Although studies have reported proteomic and transcriptomic responses within the psyllid midgut after CLAs infection, these analyses have been limited and have not examined correlated expression profiles in relation to CLAs infection. With a comprehensive psyllid RNAseq data from the Citrus Greening Expression Network (CGEN), a total of 743 genes (Official Gene Set v3, OGSv3) were determined as differentially expressed genes (DEGs) in response to CLAs infection. Forty-one modules of co-expressed genes were identified using a weighted gene co-expression network analysis (WGCNA). The functional analysis of infection-associated modules showed that genes involved in muscle contraction, peptidase and iron binding activities were correlated, which may correspond to enhanced vector dispersal, altered feeding/digestion, and sequestering free iron. Additional associated modules identified that Golgi apparatus and endoplasmic reticulum processes may be a signal indicating altered intracellular protein consumption during infection. This study provides a novel understanding of molecular mechanisms involved in CLAs-psyllid interaction which can be potential targets for disrupting CLAs transmission.

Keywords: Asian citrus psyllid; Huanglongbing; DEGs; weighted gene co-expression analysis; functional enrichment analysis; citrus; citrus greening; pathogen; expression networks; co-expression

1. Introduction

Asian citrus psyllid (ACP, *Diaphorina citri*) feeds on phloem, where it serves as a vector for *Candidatus Liberibacter asiaticus* (CLAs). This bacterium serves as an agent for citrus greening disease (Huanglongbing, HLB). Infected nymphs feed and spread CLAs quickly as individuals move through the tree. The bacteria will eventually move to the roots, causing systemic infection of the citrus tree, and this phenomenon usually precedes any symptoms [1]. 14/2022 6:07:00 PM. Often an infected tree will serve as a source of inoculum for surrounding trees for months before infection is confirmed.

There is no cure for citrus greening disease. Infected trees are asymptomatic in the early stages [2]. The time of symptom onset of different species varies from a few months to several years after infection [3]. Trees infected by HLB have many significant symptoms as the infection becomes systemic, such as leaf chlorosis, dead shoots, fruit shedding,

deformed small fruits, and reduced internal fruit quality [4], which ultimately leads to tree death and huge economic losses.

Network method applications have grown rapidly in bioinformatics to better understand interacting genes and more subtle gene expression profile differences. Weighted gene co-expression network analysis (WGCNA) has a unique advantage in identifying and understanding complex molecular interactions. In specific, this method has proven useful for the identification of specific correlated transcriptional changes that have been overlooked using other methods for RNA-seq analyses, allowing the identification of new drug targets or responses to specific factors [5].

In this study, WGCNA was used to detect the dominant genes and modules which are closely related to response to CLas infection in the psyllid gut. This was followed by standard RNA-seq analyses using DESeq2 for comparison to the WGCNA. These analyses were followed by Gene Ontology (GO) enrichment and metabolic pathway analysis that showed upregulation of gene groups associated with psyllid muscle movement, peptidase activity, and the COPI-dependent Golgi-to-ER retrograde traffic pathway.

2. Methods

2.1. RNAseq Data Set

A comprehensive RNAseq data set was acquired from the Citrus Greening Expression Network (CGEN) and used to analyze tissue-specific transcriptional data sets of adult psyllid intestine from two citrus hosts (*C. medica* and *Citrus* spp.) in relation to infection status [6,7]. Weighted gene co-expression network analysis and functional enrichment analysis of co-expression genes were conducted based on *D. citri* genes (Official Gene Set v3, OGSv3) with 21,345 genes [7]. Gene expression values were obtained after mapping RNAseq reads with HISAT2 [8] and quantified by StringTie using the transcripts per million reads (TPM) metric.

2.2. Weighted Gene Co-Expression Analysis (WGCNA)

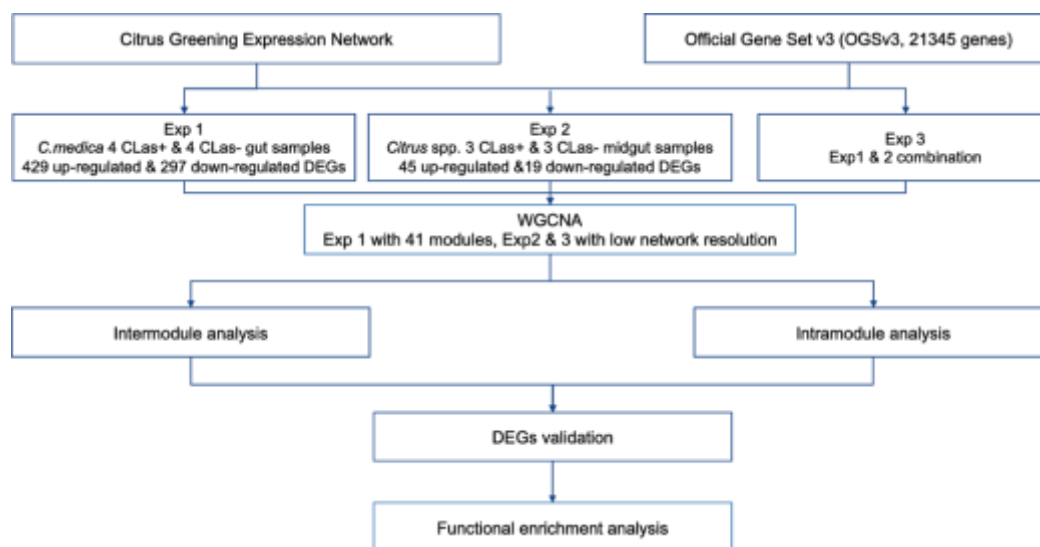


Figure 1. Weighted Gene Co-expression Analysis (WGCNA) based pipeline applied to transcriptomics data from the gut of psyllids reared on *C. medica* (Experiment 1) and *Citrus* spp. (Experiment 2). Experiment 3 was the combined data set.

2.3. Gene Module Detection and Differential Gene Expression

We filtered out 1750 genes with low variance among the samples as the input for network construction. The best estimation for signed network soft thresholding was 16 in experiment 1 (Figure 1). Then multiple co-expression modules were obtained by dynamic tree-cutting based on TOM clustering analysis [9]. DESeq2 version 1.30.1 [10] was used to

determine if the observed difference in expression counts is significant between CLAs-infected and CLAs-free samples. The significantly differential expressed genes (p -value < 0.01, fold change > 1) were also compared with WGCNA gene in main modules with R package UpSetR version 1.4.0 [11]. A WGCNA embedded function was applied to obtain the hub gene which summarizes a module with its high node connectivity [12]. Three specific previous experiments were analyses. Experiment 1 consisted of four CLAs infected and four healthy psyllid gut samples from host *C. medica*, Experiment 2 consisted of three CLAs infected and three healthy psyllid midgut samples from host *Citrus* spp., and Experiment 3 was the combination of Experiment 1 and Experiment 2.

2.4. Functional Annotation and Enrichment

Using a pipeline of functional annotation provided by AgBase [13,14], GOanna, InterProScan and KOBAS were used to transfer Gene Ontology (GO) and pathway functional annotations to the *Diaphorina citri* genes. GO functional enrichment analysis was carried out with R package topGO [15] (version 2.42) with a Fisher exact test (p -value < 0.05). Pathway enrichment analysis was obtained by KOBAS based on a Fisher exact test (p -value < 0.05).

3. Results

3.1. WGCNA for *C. medica* Psyllid Gut Transcriptome

In Experiment 1, we detected 41 modules. The sizes for the two largest modules (turquoise and blue) were 5364 and 3735 respectively. Intermodule correlations were visualized using a heatmap where the dendrogram branch tips are module names and the heatmap describes the intermodule connectivity (Figure 2). We then compared the sample’s first principle component expression level in each module. Though the original samples were derived from two conditions (CLAs infected and CLAs-free), variance among replicates was found in most of the detected modules (38/41). Only “turquoise” and “blue” modules had consistent expression levels between replicates in control and infected samples with the pink modules still showing variation (Supplementary figure 1). Therefore, we decided to examine “turquoise” and “blue” modules for genes or pathways involved in response to CLAs infection.

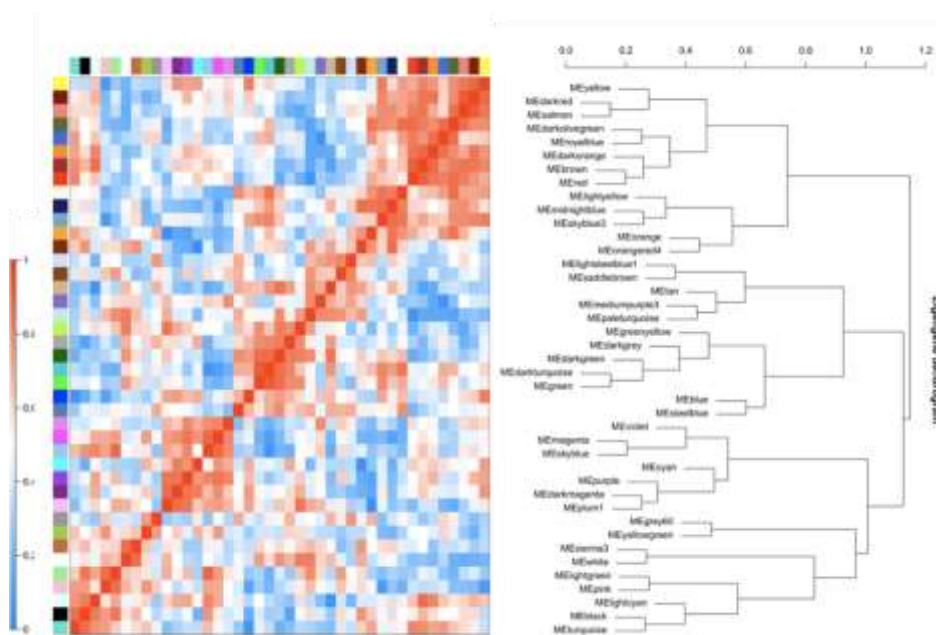


Figure 2. Intermodule dendrogram and its corresponding heatmap. Each tip of the dendrogram represents a specific module from WGCNA of transcriptome of the psyllid gut reared on *C. medica* in response to CLAs infection (Experiment 1) and the heatmap diagonal represents correlation=1.

3.2. Differential Expression and Functional Enrichment

We then applied DEG analysis to identify genes in the correlated modules that are also differentially expressed in response to CLas infection. Blue module has the largest proportion of DEGs (421/743, 56.7%) among all modules (Supplementary figure 2). By comparing the significant GO annotations between DEGs and blue module genes, we found peptidase activity and iron-related transport activity based on both analyses (Supplementary table 2). Previous evidence has shown that psyllid limits its free form iron transport for CLas iron starvation [16]. Our GO term enrichment supported this evidence especially with the ferric iron binding function (p -value = 0.01659). We also found association with muscle contraction (Table 1) and peptidase activity (Supplementary table 1). Within the cellular component ontology, troponin complex, striated muscle thin filament, myofibril and sarcomere are all significantly annotated GO terms with 80% (p -value=0.0087) enrichment. The blue module was mainly involved in metabolism-related pathways (p -value < 0.05) while the genes in the turquoise module are related to transcription-related pathways (Supplementary table 3).

Table 1. Functional profiles in cellular component ontology for blue module in Experiment 1 containing 4 CLas infected and 4 CLas free psyllid gut samples collected from *C.medica*.

GO.ID	Term	Annotated ¹	Significant ²	Expected ³	Classic ⁴
GO:0005861	troponin complex	5	4	1.06	0.0084
GO:0015629	actin cytoskeleton	87	27	18.49	0.0201
GO:0005865	striated muscle thin filament	6	4	1.28	0.021
GO:0036379	myofilament	6	4	1.28	0.021

¹Annotated represents annotated genes with certain GO term among the whole genome

²Significant represents the annotated genes with certain GO term among blue module

³Expected represents the expected genes to be annotated with certain GO term

⁴Classic represents the Fisher Exact test p -value

For further assessment of the blue module, we analyzed the functional profile of the hub gene. Dcitr02g08650.1.1 is involved in Golgi-to-ER retrograde traffic activity and also contains the kinesin motor domain related to microtubule-based movement. This indicates this hub gene may induce ER vesicles recycling molecules back from Golgi complex to ER in the cytoplasm.

3.3. Low Network Connectivity for Other Experiments

We analyzed the weighted gene co-expression network of Experiment 2 and 3 (Figure 1), which detected 15 and 25 modules respectively. However, the constructed network showed relatively low conformation to the scale-free network characteristics. Experiment 2 showed lower than 60% model fitness (Supplementary figure 5). Due to the differences of host plant species among samples in Experiment 1 and 2, there was no significant difference in transcriptome expression between the CLas infected and CLas-free psyllids in the multi-sample groups for principal component analysis (Supplementary figure 6) for Experiment 3. The primary driver for psyllid gene expression was the citrus host (Supplementary figure 6) with a 57% variance among the samples irrespective of CLas infection status. Comparing the up and down regulated DEGs (p -value < 0.01) between Experiment 1 and 2, the common genes were few (Figure 3). As a result, the network model fitness in Experiment 3 was lower than 70% in comparison to Experiment 1 which was 90%.

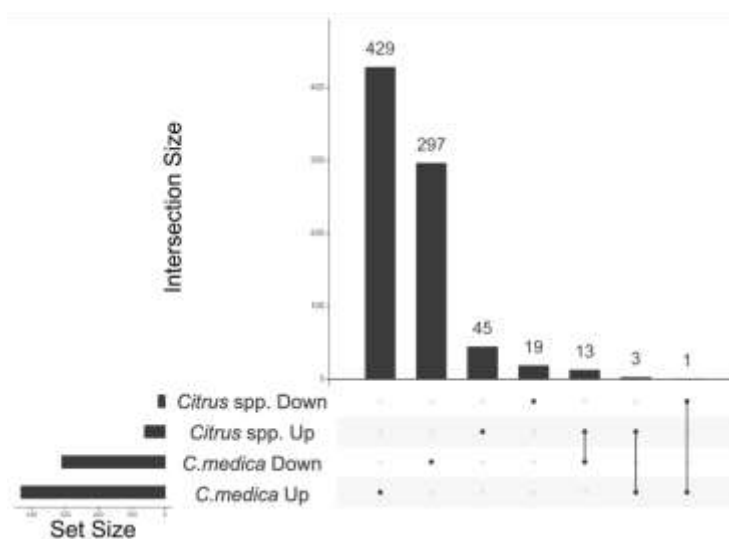


Figure 3. Upset plot for DEGs comparison between Experiment 1 and 2. Few common DEGs were found between Experiment 1 and 2. The largest overlap was between down regulated DEGs in Experiment 1 and up regulated DEGs in Experiment 2.

4. Discussion

In this study, we constructed a weighted gene co-expression network to detect the genes that are co-expressed in response to the CLAs infection in the gut of the Asian citrus psyllid. We identified that psyllid muscle movement, peptidase activity and iron binding are associated with infection. The hub gene was annotated as participating in intracellular cargo transportation. In the following section, we will discuss gene modules with correlated expression in response to CLAs infection and citrus host-specific response in psyllid to CLAs infection.

4.1. Enhanced Muscle Movement, Free Amino Acid Production and Iron Binding in Response of CLAs Infection

We found muscle associated GO terms from the cellular component ontology in the blue module. A contraction within cross-striated flight muscle is the result of a single sarcomere binding of Ca^{2+} on troponin C within the troponin complex where it displaces tropomyosin from actin (thin filament). Myosin finally ratchets with actin and shortens sarcomeres leading to muscle contraction [17]. Hence, we hypothesize that the blue module might be involved in changes in psyllid dispersal after CLAs infection. It has been reported that CLAs infection enhances CLAs transmission by strengthening psyllid dispersal ability and increasing its flight initiation frequency [18].

Peptidase activity is significantly present in annotated proteins in the blue module and may indicate the production of free amino acid which could be utilized by CLAs. Previous study shows evidence that CLAs-infected psyllids had higher expression of haemocyanin, an amino acid storage and energy-supplying protein, together with detection of more derived peptides from it [19]. Compared to the low adulthood haemocyanin expression in CLAs free healthy psyllids, our enhanced peptidase activity revealed the increased energy stress in CLAs infected adult psyllids, which might be associated with more feeding that will promote transfer of CLAs to more citrus hosts.

Moreover, the hub gene of the blue module (Dcitr02g08650.1.1, Table 3) is related to the microtubule-based movement and contains the kinesin domain. It also participates in the COPI-dependent Golgi-endoplasmic reticulum retrograde transport and kinesin pathway. Kinesin is a motor protein traveling along microtubules and harnessing energy from ATP [20]. Different from most kinesins, motor proteins transport cargo to the nucleus. This retrograde transport is regulated by microtubule-directed COPI-coated vesicles [21,22]. This retrieval is also part of the compensatory process to maintain the homeostasis

of the Golgi complex as ER-to-Golgi is the major secretory step in intracellular cargo transportation [23]. At the same time, a large amount of intracellular cargo transport also increases the pressure on the ATP metabolism of psyllids, which may also explain that infected psyllids are at a high hunger level, tend to forage more and their environmental resilience is greatly reduced [24].

In the bacteria-host interaction, the host iron binding complexes are usually the source for maintaining bacteria iron homeostasis [25]. The foliar Fe application restored the infected citrus symptoms in previous findings indicating iron nutrition preference in CLAs [26]. With an incomplete immune system, psyllid relies on co-evolved alternatives to limit CLAs amplification [6,27]. Proteomic evidence has shown that iron binding protein is upregulated after CLAs infection [6]. The consistency between enhanced ferric iron binding process from WGCNA and previous evidence suggests that psyllid sequesters the body free iron limiting the CLAs proliferation.

4.2. Citrus Host-Specific Psyllid Response to CLAs Infection

Host-specific psyllid responses are a common observation in vector biology experiments and provide evidence for integrated pest management strategies customized to the local or regional pathosystem. It has been reported that volatile organic compounds (VOC) such as methyl salicylate released by certain citrus species altered the host-choice behavior in psyllids [28]. Furthermore, the nutrient element differences between infected but attractive citrus and healthy citrus [29] implies that the citrus host nutrient level may also be a factor in the host-specific response. Both factors affect the attractiveness of the citrus host for psyllid and eventually influence the CLAs transmission rate. In Experiment 3, when we combined psyllid gut transcripts from citrus hosts with distinct psyllid attractiveness, a significant host specific variance was introduced into analysis, which was detrimental for network connectivity and led to poor network model fitness.

5. Conclusion

In this study, we identified a co-expressed psyllid gene module in response to CLAs infection, which promoted psyllid muscle movement, peptidase and iron binding activities. Its hub gene (Dcitr02g08650.1.1) was involved in the Golgi-to-ER retrograde traffic activity and contains the kinesin motor domain related to intracellular cargo transport. Both results suggest that these genes are of interest for the study of the response to CLAs infection in psyllid guts. Our study provides new insights into the complex regulatory mechanisms of psyllid response to CLAs infection using network analysis. Further work will be done to apply differential expression and WGCNA to transcriptomes from additional tissues and citrus hosts with a goal to identify host-specific solutions to citrus greening in *D. citri*.

Supplementary Materials: The following are available online at <https://figshare.com/s/9678da9a91f448e4b62a>, Abbreviations, Supplementary table 1, Supplementary table 2, Supplementary figure 1, Supplementary figure 2, Supplementary figure 3, Supplementary figure 4, Supplementary figure 5.

Author Contributions: Conceptualization, S.S and C.C.; methodology, C.C, S.S. and J.B.; software, C.C.; validation, S.S and J.B.; formal analysis, C.C.; investigation, C.C.; resources, S.S and C.C.; writing—original draft preparation, C.C.; writing—review and editing, S.S. and J.B.; visualization, C.C.; supervision, S.S.; project administration, S.S and L.M.; funding acquisition, L.M and S.S. All authors have read and agreed to the published version of the manuscript.

Funding: This research was funded by USDA-NIFA grant 2015-70016-23028, HSI 1300394, 2020-70029-33199.

Data Availability Statement: The WGCNA results and related annotation files are accessible via the Citrus Greening website (<https://citrusgreening.org/>).

Conflicts of Interest: The authors declare no conflict of interest. The funders had no role in the design of the study; in the collection, analyses, or interpretation of data; in the writing of the manuscript, or in the decision to publish the results.

Appendix A

Abbreviations

Abbreviations	Full term
ACP	Asian citrus psyllid
CLas	<i>Candidatus Liberibacter asiaticus</i>
WGCNA	Weighted gene co-expression network analysis
CGEN	Citrus Greening Expression Network
OGSv3	Official Gene Set v3
HLB	Huanglongbing
GO	Gene ontology
<i>C. medica</i>	<i>Citrus medica</i>
ER	Endoplasmic reticulum

Supplementary table 1. Functional profiles for blue modules in Experiment 1

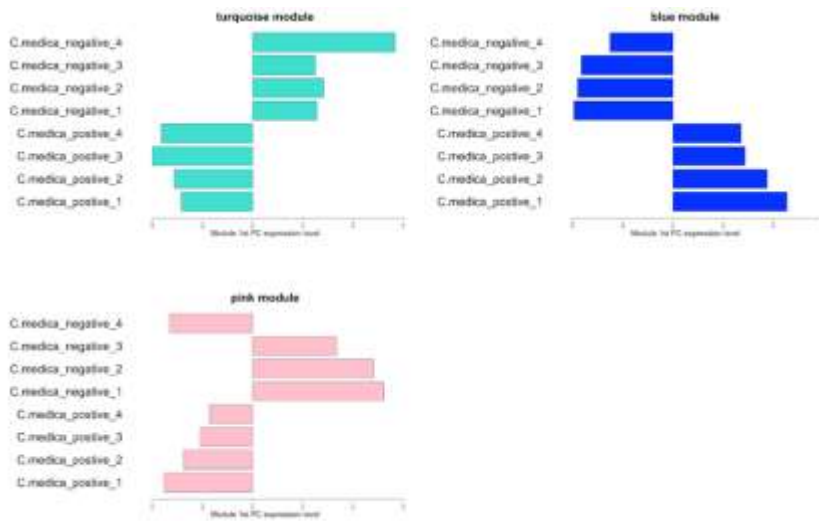
GO.ID	Term abbr.	Annotated	Significant	Expected	Classic	Ontology
GO:0043603	cellular amide metabolic process	449	128	93.74	4.60E-05	biological process
GO:0046916	cellular transition metal ion homeostasi...	10	8	2.09	0.00011	
GO:0043604	amide biosynthetic process	409	114	85.39	0.00032	
GO:0006518	peptide metabolic process	414	115	86.44	0.00035	
GO:0044281	small molecule metabolic process	566	150	118.17	0.0005	
GO:0006412	translation	381	106	79.55	0.00056	
GO:0055076	transition metal ion homeostasis	12	8	2.51	0.00078	
GO:0034470	ncRNA processing	139	45	29.02	0.00093	
GO:0043043	peptide biosynthetic process	391	107	81.64	0.00099	
GO:0034660	ncRNA metabolic process	212	63	44.26	0.00129	
GO:1901566	organonitrogen compound biosynthetic pro...	697	176	145.52	0.00196	
GO:0015074	DNA integration	44	18	9.19	0.00197	
GO:0006396	RNA processing	361	98	75.37	0.0021	
GO:0006508	proteolysis	541	140	112.95	0.00213	
GO:0022613	ribonucleoprotein complex biogenesis	127	40	26.52	0.00306	

GO:0000041	transition metal ion transport	14	8	2.92	0.00317		
GO:0046112	nucleobase biosynthetic process	14	8	2.92	0.00317		
GO:0042254	ribosome biogenesis	88	29	18.37	0.00535		
GO:0051347	positive regulation of transferase activ...	21	10	4.38	0.00557	Cellular component	
GO:0005840	ribosome	227	67	48.25	0.0016		
GO:0005861	troponin complex	5	4	1.06	0.0084		
GO:0005773	vacuole	20	9	4.25	0.0147		
GO:0032991	protein-containing complex	1299	303	276.13	0.0157		
GO:0005743	mitochondrial inner membrane	74	24	15.73	0.016		
GO:0015629	actin cytoskeleton	87	27	18.49	0.0201		
GO:0005865	striated muscle thin filament	6	4	1.28	0.021		
GO:0031082	BLOC complex	6	4	1.28	0.021		
GO:0031083	BLOC-1 complex	6	4	1.28	0.021		
GO:0031414	N-terminal protein acetyltransferase com...	6	4	1.28	0.021		
GO:0036379	myofilament	6	4	1.28	0.021		
GO:0033588	Elongator holoenzyme complex	9	5	1.91	0.0251		
GO:0048500	signal recognition particle	9	5	1.91	0.0251		
GO:1905354	exoribonuclease complex	9	5	1.91	0.0251		
GO:0019866	organelle inner membrane	77	24	16.37	0.026		
GO:0043228	non-membrane-bounded organelle	629	151	133.71	0.0389		
GO:0043232	intracellular non-membrane-bounded organ...	629	151	133.71	0.0389		
GO:0019005	SCF ubiquitin ligase complex	7	4	1.49	0.0409		
GO:0005798	Golgi-associated vesicle	20	8	4.25	0.0443		
GO:0016742	hydroxymethyl-	9	7	1.79	0.0003		Molecular Function
GO:0003735	structural constituent of ribosome	228	66	45.35	0.00058		
GO:0005198	structural molecule activity	369	99	73.4	0.00061		
GO:0008233	peptidase activity	477	123	94.88	0.00077		
GO:0008234	cysteine-type peptidase activity	76	26	15.12	0.00235		
GO:1901682	sulfur compound transmembrane transporte...	21	10	4.18	0.00386		
GO:0008271	secondary active sulfate transmembrane t...	19	9	3.78	0.00636		
GO:0015116	sulfate transmembrane transporter activi...	19	9	3.78	0.00636		
GO:0004615	phosphomannomutase activity	3	3	0.6	0.00786		
GO:0004637	phosphoribosylamine-glycine ligase activ...	3	3	0.6	0.00786		

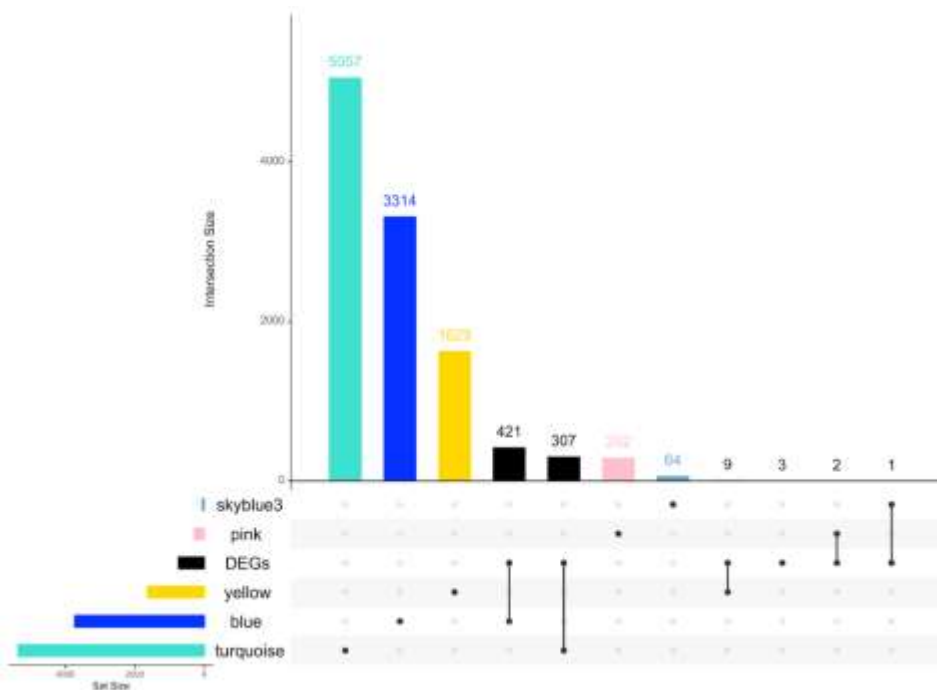
GO:0016627	oxidoreductase activity	41	15	8.16	0.00956
GO:0000049	tRNA binding	14	7	2.78	0.0112
GO:0140101	catalytic activity	97	29	19.29	0.01183
GO:0030234	enzyme regulator activity	160	44	31.83	0.01189
GO:0070008	serine-type exopeptidase activity	24	10	4.77	0.01204
GO:0004185	serine-type carboxypeptidase activity	18	8	3.58	0.01567
GO:0003824	catalytic activity	4344	905	864.08	0.01645
GO:0003997	acyl-CoA oxidase activity	6	4	1.19	0.01659
GO:0005337	nucleoside transmembrane transporter act...	6	4	1.19	0.01659

Supplementary table 2 Functional profiles for intersection genes between blue modules and DEGs in Experiment 1

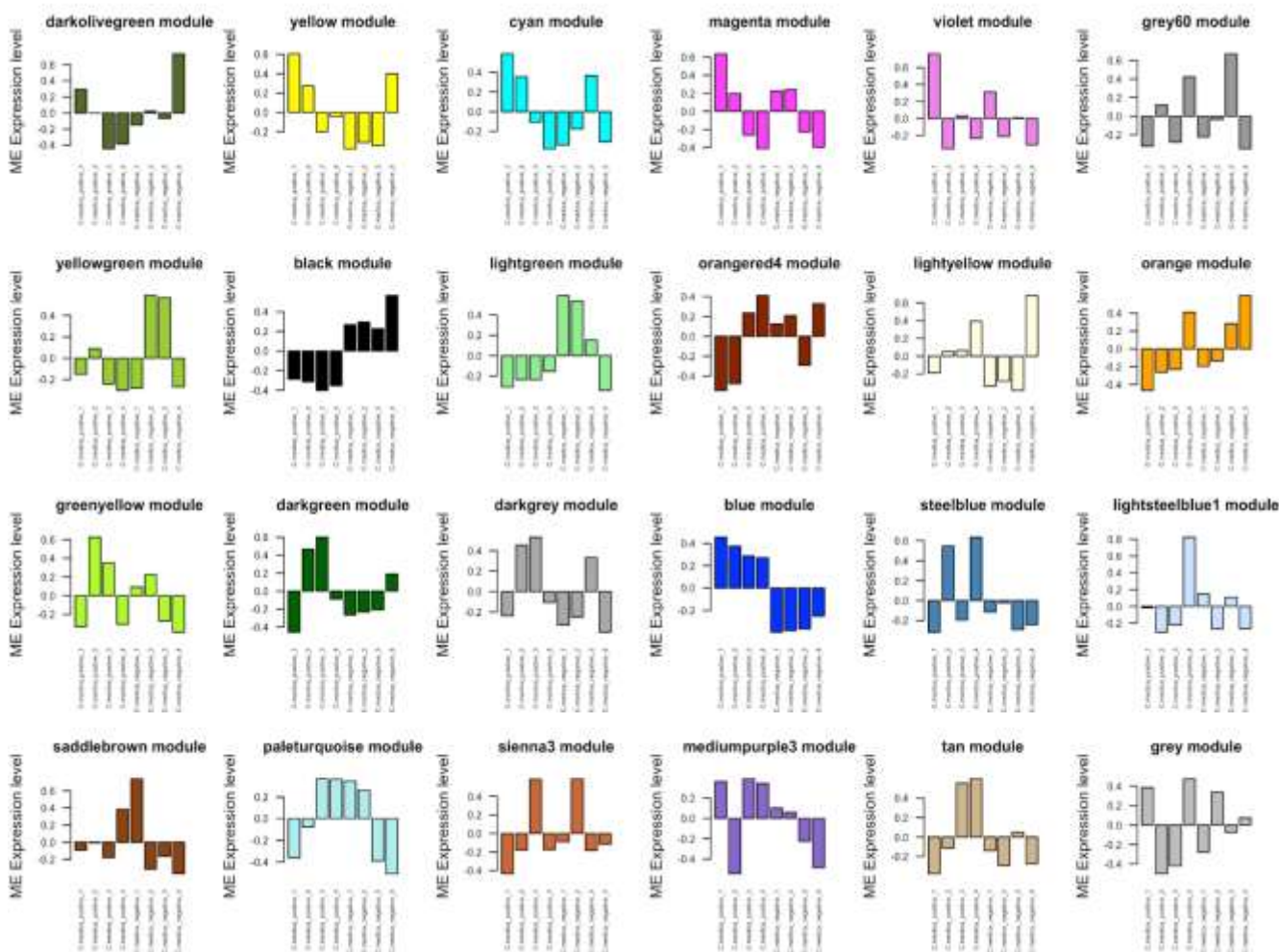
GO.ID	Term	Annotated	Significant	Expected	Classic	Ontology
GO:0006518	peptide metabolic process	414	36	12.1	2.40E-09	Biological process
GO:0043043	peptide biosynthetic process	391	33	11.43	2.50E-08	
GO:1901566	organonitrogen compound biosynthetic pro...	697	45	20.38	2.10E-07	
GO:0006826	iron ion transport	7	5	0.2	4.10E-07	
GO:0006879	cellular iron ion homeostasis	7	4	0.2	2.30E-05	
GO:0000041	transition metal ion transport	14	5	0.41	3.30E-05	
GO:0055072	iron ion homeostasis	8	4	0.23	4.50E-05	
GO:0005840	ribosome	227	32	7.77	1.60E-12	Cellular component
GO:0043232	intracellular non-membrane-bounded organ...	629	38	21.52	0.00019	
GO:0043228	non-membrane-bounded organelle	629	38	21.52	0.00019	
GO:0031090	organelle membrane	257	18	8.79	0.00258	
GO:0019866	organelle inner membrane	77	8	2.63	0.00441	
GO:0003735	structural constituent of ribosome	228	31	6.47	2.40E-13	Molecular function
GO:0005198	structural molecule activity	369	35	10.47	2.40E-10	
GO:0008199	ferric iron binding	6	4	0.17	9.10E-06	
GO:0004185	serine-type carboxypeptidase activity	18	5	0.51	0.00011	
GO:0070008	serine-type exopeptidase activity	24	5	0.68	0.00048	
GO:0008238	exopeptidase activity	58	7	1.65	0.00119	
GO:0050661	NADP binding	20	3	0.57	0.01803	



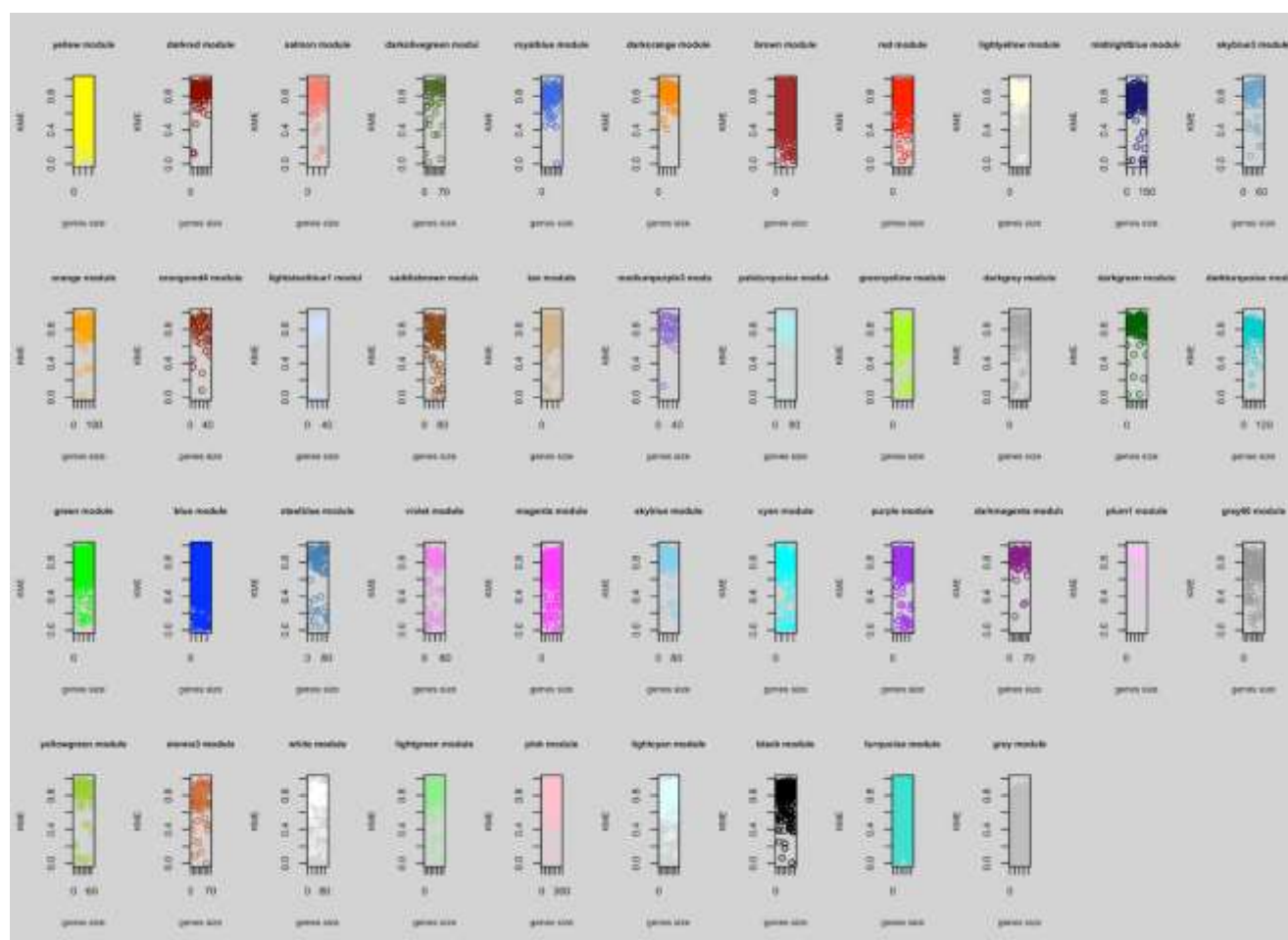
Supplementary figure 1 First principle component expression level among the modules between 8 samples (*C. medica* host, CLas-infected and CLas free) in “turquoise”, “blue” and “pink” modules. “Turquoise” and “blue” modules had consistent expression levels between replicates in control and infected samples with the pink modules showing variation.



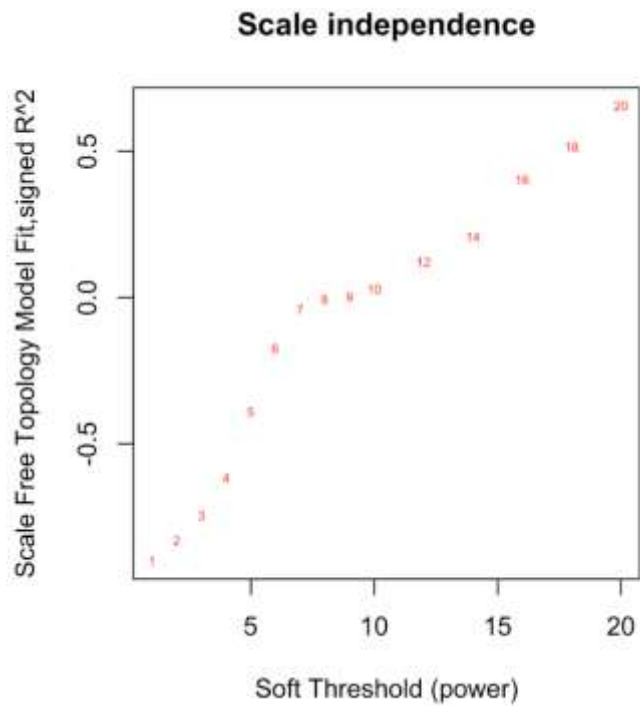
Supplementary figure 2 Upset plot of DEGs and module genes intersection in the Experiment 1. Turquoise module has the largest module size but blue module has the greatest number of DEGs (forth black bar) among all the detected modules. Yellow and sky-blue3 modules have few DEGs corresponding to their lower module size.



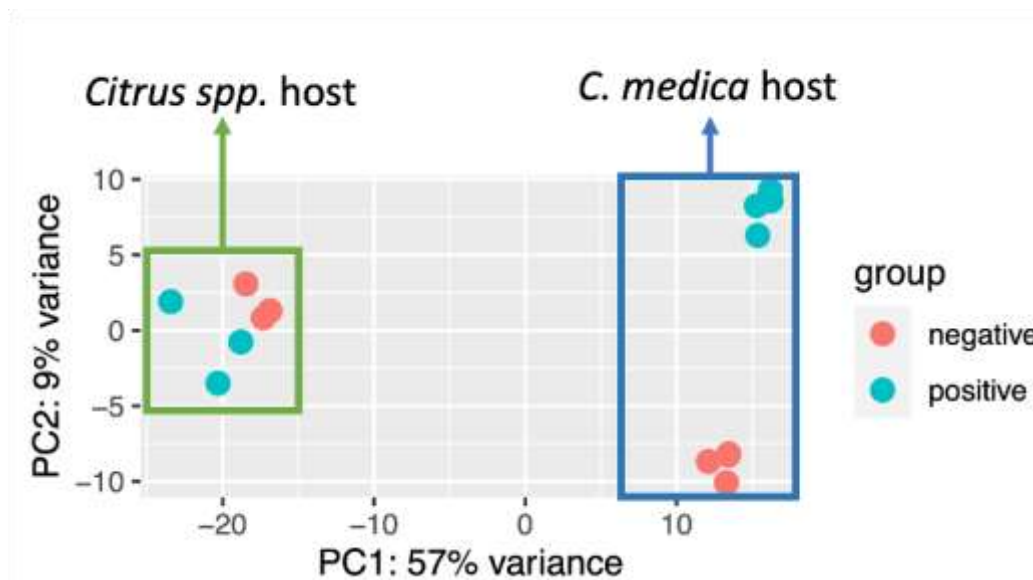
Supplementary figure 3 Average expression level among the 41 modules between total 8 samples in the Experiment 1. Besides “Turquoise” and “blue” modules, other modules all showed variation in expression levels between replicates in control and infected samples. Here grey module was a collection of low connectivity genes among the genome with few biological meaning.



Supplementary figure 4 Intramodule genes connectivity in the Experiment 1 in 41 modules. Here most of modules were showing high gene connectivity within the module except grey module which was a collection of low connectivity genes among the genome with few biological meaning.



Supplementary figure 5 Experiment 2 Soft thresholding picking while the scale free topology model fit is low ($R^2 < 0.6$)



Supplementary figure 6 PCA plot for Experiment 3 samples. No significant difference in transcriptome expression between the CLAs infected and CLAs-free psyllids in the multi-sample groups of eight CLAs infected and healthy psyllid gut sample from *C. medica* host and six CLAs infected and healthy psyllid midgut sample from *Citrus spp.*.

References

- Louzada, E.S.; Vazquez, O.E.; Braswell, W.E.; Yanev, G.; Devanaboina, M.; Kunta, M. Distribution of ‘Candidatus Liberibacter Asiaticus’ Above and Below Ground in Texas Citrus. *Phytopathology*® **2016**, *106*, 702–709, doi:10.1094/PHYTO-01-16-0004-R.
- Lee, J.A.; Halbert, S.E.; Dawson, W.O.; Robertson, C.J.; Keesling, J.E.; Singer, B.H. Asymptomatic Spread of Huanglongbing and Implications for Disease Control. *Proc. Natl. Acad. Sci.* **2015**, *112*, 7605–7610, doi:10.1073/pnas.1508253112.
- Gottwald, T.R. Citrus Canker and Citrus Huanglongbing, Two Exotic Bacterial Diseases Threatening the Citrus Industries of the Western Hemisphere. *Outlooks Pest Manag.* **2007**, *18*, 274–279, doi:http://dx.doi.org/10.1564/18dec09.
- Dala-Paula, B.M.; Plotto, A.; Bai, J.; Manthey, J.A.; Baldwin, E.A.; Ferrarezi, R.S.; Gloria, M.B.A. Effect of Huanglongbing or Greening Disease on Orange Juice Quality, a Review. *Front. Plant Sci.* **2019**, *9*, doi:10.3389/fpls.2018.01976.
- He, D.; Liu, Z.-P.; Honda, M.; Kaneko, S.; Chen, L. Coexpression Network Analysis in Chronic Hepatitis B and C Hepatic Lesions Reveals Distinct Patterns of Disease Progression to Hepatocellular Carcinoma. *J. Mol. Cell Biol.* **2012**, *4*, 140–152, doi:10.1093/jmcb/mjs011.
- Kruse, A.; Fattah-Hosseini, S.; Saha, S.; Johnson, R.; Warwick, E.; Sturgeon, K.; Mueller, L.; MacCoss, M.J.; Shatters, R.G.; Cilia Heck, M. Combining ‘omics and Microscopy to Visualize Interactions between the Asian Citrus Psyllid Vector and the Huanglongbing Pathogen Candidatus Liberibacter Asiaticus in the Insect Gut. *PLOS ONE* **2017**, *12*, e0179531, doi:10.1371/journal.pone.0179531.
- Flores-Gonzalez, M.; Hosmani, P.S.; Fernandez-Pozo, N.; Mann, M.; Humann, J.L.; Main, D.; Heck, M.; Brown, S.; Mueller, L.A.; Saha, S. Citrusgreening.Org: An Open Access and Integrated Systems Biology Portal for the Huanglongbing (HLB) Disease Complex. **2019**, doi:10.1101/868364.
- Kim, D.; Paggi, J.M.; Park, C.; Bennett, C.; Salzberg, S.L. Graph-Based Genome Alignment and Genotyping with HISAT2 and HISAT-Genotype. *Nat. Biotechnol.* **2019**, *37*, 907–915, doi:10.1038/s41587-019-0201-4.
- Zhang, B.; Horvath, S. A General Framework for Weighted Gene Co-Expression Network Analysis. *Stat. Appl. Genet. Mol. Biol.* **2005**, *4*, doi:10.2202/1544-6115.1128.
- Love, M.I.; Huber, W.; Anders, S. Moderated Estimation of Fold Change and Dispersion for RNA-Seq Data with DESeq2. *Genome Biol.* **2014**, *15*, 550, doi:10.1186/s13059-014-0550-8.
- Conway, J.R.; Lex, A.; Gehlenborg, N. UpSetR: An R Package for the Visualization of Intersecting Sets and Their Properties. *Bioinformatics* **2017**, *33*, 2938–2940, doi:10.1093/bioinformatics/btx364.
- Langfelder, P.; Horvath, S. WGCNA: An R Package for Weighted Correlation Network Analysis. *BMC Bioinformatics* **2008**, *9*, 559, doi:10.1186/1471-2105-9-559.
- McCarthy, F.M.; Wang, N.; Magee, G.B.; Nanduri, B.; Lawrence, M.L.; Camon, E.B.; Barrell, D.G.; Hill, D.P.; Dolan, M.E.; Williams, W.P.; et al. AgBase: A Functional Genomics Resource for Agriculture. *BMC Genomics* **2006**, *7*, 229, doi:10.1186/1471-2164-7-229.
- McCarthy, F.M.; Bridges, S.M.; Wang, N.; Magee, G.B.; Williams, W.P.; Luthe, D.S.; Burgess, S.C. AgBase: A Unified Resource for Functional Analysis in Agriculture. *Nucleic Acids Res.* **2007**, *35*, D599–D603, doi:10.1093/nar/gk1936.
- Alexa, A.; Rahnenfuhrer, J.; Lengauer, T. Improved Scoring of Functional Groups from Gene Expression Data by Decorrelating GO Graph Structure. *Bioinformatics* **2006**, *22*, 1600–1607, doi:10.1093/bioinformatics/btl140.
- Vyas, M.; Fisher, T.W.; He, R.; Nelson, W.; Yin, G.; Cicero, J.M.; Willer, M.; Kim, R.; Kramer, R.; May, G.A.; et al. Asian Citrus Psyllid Expression Profiles Suggest Candidatus Liberibacter Asiaticus-Mediated Alteration of Adult Nutrition and Metabolism, and of Nymphal Development and Immunity. *PLOS ONE* **2015**, *10*, e0130328, doi:10.1371/journal.pone.0130328.
- Iwamoto, H. Structure, Function and Evolution of Insect Flight Muscle. *Biophys. Nagoya-Shi Jpn.* **2011**, *7*, 21–28, doi:10.2142/biophysics.7.21.
- Martini, X.; Hoffmann, M.; Coy, M.R.; Stelinski, L.L.; Pelz-Stelinski, K.S. Infection of an Insect Vector with a Bacterial Plant Pathogen Increases Its Propensity for Dispersal. *PLOS ONE* **2015**, *10*, e0129373, doi:10.1371/journal.pone.0129373.
- Ramsey, J.S.; Chavez, J.D.; Johnson, R.; Hosseinzadeh, S.; Mahoney, J.E.; Mohr, J.P.; Robison, F.; Zhong, X.; Hall, D.G.; MacCoss, M.; et al. Protein Interaction Networks at the Host–Microbe Interface in Diaphorina Citri, the Insect Vector of the Citrus Greening Pathogen. *R. Soc. Open Sci.* **2017**, *4*, doi:10.1098/rsos.160545.
- Berg, J.M.; Tymoczko, J.L.; Stryer, L.; Berg, J.M.; Tymoczko, J.L.; Stryer, L. *Biochemistry*; 5th ed.; W H Freeman, 2002; ISBN 978-0-7167-3051-4.
- Lord, T.; Aitken, R.J. Oxidative Stress and Ageing of the Post-Ovulatory Oocyte. *Reproduction* **2013**, *146*, R217–R227, doi:10.1530/REP-13-0111.
- Spang, A. Retrograde Traffic from the Golgi to the Endoplasmic Reticulum. *Cold Spring Harb. Perspect. Biol.* **2013**, *5*, a013391, doi:10.1101/cshperspect.a013391.
- Cancino, J.; Jung, J.E.; Luini, A. Regulation of Golgi Signaling and Trafficking by the KDEL Receptor. *Histochem. Cell Biol.* **2013**, *140*, 395–405, doi:10.1007/s00418-013-1130-9.
- Killiny, N.; Nehela, Y. Metabolomic Response to Huanglongbing: Role of Carboxylic Compounds in Citrus Sinensis Response to ‘Candidatus Liberibacter Asiaticus’ and Its Vector, Diaphorina Citri. *Mol. Plant-Microbe Interactions*® **2017**, *30*, 666–678, doi:10.1094/MPMI-05-17-0106-R.
- Andrews, S.C.; Robinson, A.K.; Rodríguez-Quñones, F. Bacterial Iron Homeostasis. *FEMS Microbiol. Rev.* **2003**, *27*, 215–237, doi:10.1016/S0168-6445(03)00055-X.

26. Inoue, H.; Yamashita-Muraki, S.; Fujiwara, K.; Honda, K.; Ono, H.; Nonaka, T.; Kato, Y.; Matsuyama, T.; Sugano, S.; Suzuki, M.; et al. Fe²⁺ Ions Alleviate the Symptom of Citrus Greening Disease. *Int. J. Mol. Sci.* **2020**, *21*, doi:10.3390/ijms21114033.
27. Arp, A.P.; Hunter, W.B.; Pelz-Stelinski, K.S. Annotation of the Asian Citrus Psyllid Genome Reveals a Reduced Innate Immune System. *Front. Physiol.* **2016**, *7*, doi:10.3389/fphys.2016.00570.
28. Nehela, Y.; Hijaz, F.; Elzaawely, A.A.; El-Zahaby, H.M.; Killiny, N. Citrus Phytohormonal Response to Candidatus Liberibacter Asiaticus and Its Vector Diaphorina Citri. *Physiol. Mol. Plant Pathol.* **2018**, *102*, 24–35, doi:10.1016/j.pmpp.2017.11.004.
29. Patt, J.M.; Robbins, P.S.; Niedz, R.; McCollum, G.; Alessandro, R. Exogenous Application of the Plant Signalers Methyl Jasmonate and Salicylic Acid Induces Changes in Volatile Emissions from Citrus Foliage and Influences the Aggregation Behavior of Asian Citrus Psyllid (*Diaphorina Citri*), Vector of Huanglongbing. *PLOS ONE* **2018**, *13*, e0193724, doi:10.1371/journal.pone.0193724.